Magnetic and structural properties of stage-1 $NiCl_2$-graphite intercalation compounds

J. T. Nicholls
Department of Physics and Center for Materials Science and Engineering, Massachusetts Institute of Technology, Cambridge, Massachusetts 02139

J. S. Speck
Department of Materials Science and Engineering, Massachusetts Institute of Technology, Cambridge, Massachusetts 02139

G. Dresselhaus
Francis Bitter National Magnet Laboratory, Massachusetts Institute of Technology, Cambridge, Massachusetts 02139
(Received 30 December 1988)

Stage-1 $NiCl_2$-graphite intercalation compounds (GIC's) have been prepared under conditions of high temperature and high Cl_2 pressure. These compounds have a c-axis repeat distance of $I_c = 9.36 \pm 0.05$ Å, and the intercalate has a rhombohedral interplanar stacking sequence similar to pristine $NiCl_2$. Just as with stage-1 $CoCl_2$-GIC's, the magnetic behavior of stage-1 $NiCl_2$-GIC's appears always to be three dimensional. We interpret the magnetic phase transition at $T = 22.0 \pm 0.5$ K as the Néel temperature T_N. At lower temperatures, the ac susceptibility shows two magnetic field-induced transitions when a magnetic field is applied in the x-y plane. At $T = 11.5$ K, a temperature much less than T_N, the transition field values are $H_{c1} = 380$ Oe and $H_{c2} = 780$ Oe. Compared with similar measurements in stage-2 $NiCl_2$-GIC's and pristine $NiCl_2$, we estimate that the ratios of the interplanar antiferromagnetic couplings $J'_{\text{pristine}} : J'_{\text{stage}-1} : J'_{\text{stage}-2}$ are 720:24:1. These new results now provide us with two families, stage-1 and stage-2 $CoCl_2$-GIC's and $NiCl_2$-GIC's, from which some general trends about quasi-two-dimensional systems can be inferred.

I. INTRODUCTION

In this paper we report on the magnetic and structural properties of nearly pure stage-1 $NiCl_2$-GIC's (graphite intercalation compounds). This first-stage compound, which has not been investigated before in any detail, provides an important link between pristine $NiCl_2$ and stage-2 $NiCl_2$-GIC's; the latter is considered a good candidate for observing two-dimensional planar magnetic (2D XY) behavior. To facilitate the comparison of the magnetic properties of stage-1 $NiCl_2$-GIC's with other GIC's, it is useful to review the properties of $CoCl_2$-GIC's and stage-2 $NiCl_2$-GIC's, as well as their parent pristine metal chlorides.

Pristine $NiCl_2$ and $CoCl_2$ have been studied as possible XY magnets because the crystal field anisotropy favors the spins lying down in the x-y plane. In these metal chlorides, the in-plane exchange interaction J is strong and ferromagnetic, whereas the interplanar exchange interaction J' is weak and antiferromagnetic. Upon intercalation, the $NiCl_2$ and $CoCl_2$ layers retain their in-plane properties (e.g., in-plane lattice constants, in-plane exchange constants), but the interplanar parameters will be changed. A dramatic decrease of J' is expected. However small J' becomes, these systems will eventually order into a three-dimensional (3D) magnetic state at a sufficiently low temperature. Below the 3D ordering temperature, there are sheets of ferromagnetically aligned spins, and these sheets are ordered antiferromagnetically along the c axis.

Using neutron scattering, Ikeda *et al.*[1] reported that stage-1 $CoCl_2$-GIC's have a Néel temperature of 9.9 K, which is close to the upper of the two maxima that are observed in temperature-dependent ac susceptibility measurements. For the stage-1 $CoCl_2$-GIC the c-axis antiferromagnetic coherence length ξ_c is about 20 magnetic layers.[1] For the stage-2 $CoCl_2$-GIC, the three-dimensional order is found to set in at a lower temperature, $T_{cl} = 8.0$ K. At a slightly higher temperature, $T_{cu} = 9.1$ K, another magnetic transition is observed, and it is thought that in the region $T_{cl} < T < T_{cu}$, the stage-2 compound is in a 2D XY Kosterlitz-Thouless phase. Later neutron work[2] provided some support for this identification of the transition temperatures. Although the values of T_{cl} and T_{cu} vary from group to group (often using different experimental techniques to probe these magnetic properties), it is always found that the 3D ordering temperature in the stage-1 compound is higher than T_{cu} and T_{cl} of the stage-2 compound. Additionally, the 3D magnetic order in the stage-2 compound is not long range as in the stage-1 compound, ξ_c being equal to two or three layers.[2] Stage-2 $NiCl_2$-GIC's have magnetic properties[2] similar to those of stage-2 $CoCl_2$-GIC's, where the values of T_c are scaled appropriately by JS^2, with $T_{cl} \approx 18$ K and $T_{cu} \approx 21$ K. In this paper we show evidence suggesting that stage-1 $NiCl_2$-GIC's order into a 3D antiferromagnetic state at 22.0 ± 0.5 K, a temperature greater than T_{cu} for stage-2 $NiCl_2$-GIC's. This evidence is in part inferred from comparative studies with $CoCl_2$-GIC's.

 ©1989 The American Physical Society

In Sec. II of this paper we report results on the structural characterization of the new stage-1 $NiCl_2$-GIC samples and in Sec. III on magnetic investigations, including ac susceptibility, magnetotransport, and magnetization studies. The magnetic studies are preliminary because we have not yet been able to synthesize stage-1 samples with less than $\sim 10\%$ stage-2 contamination. One major objective of the magnetic experiments is to obtain an approximate value for the interplanar antiferromagnetic coupling constant J' as discussed in Sec. IV.

II. SAMPLE PREPARATION AND STRUCTURAL CHARACTERIZATION

The reaction kinetics and sample preparation conditions for stage-2 $NiCl_2$-GIC's have been extensively investigated.[3] Like other transition-metal chlorides, the intercalation reaction requires the presence of a Cl_2 atmosphere; in general, the higher the chlorine pressure P_{Cl_2}, the lower the stage obtained. In their study, Flandrois *et al.*[3] state that when the reaction temperature was raised to 690 °C, keeping P_{Cl_2} fixed at one atmosphere, it was not possible to make stage-1 $NiCl_2$-GIC's.

We have successfully made stage-1 samples using significantly higher Cl_2 pressures, about four atmospheres at room temperature, and high temperatures (660 °C), using a method previously applied to prepare stage-1 $CoCl_2$-GIC's of high staging fidelity and homogeneity.[4] The greater difficulty in making stage-1 $NiCl_2$-GIC's compared to stage-1 $CoCl_2$-GIC's is probably due to the higher melting point of the former [$T_{mp}(NiCl_2) = 1001$ °C, and $T_{mp}(CoCl_2) = 724$ °C], which causes slower kinetics at a given reaction temperature (e.g., 560 °C). Stumpp[5] has recently synthesized nominally stage-1 $NiCl_2$-GIC's starting with a stage-1 $CdCl_2$-GIC and proceeding with a displacement reaction to yield a mixed compound $C_5NiCl_2(CdCl_2)_{0.14}$; for these samples a c-axis repeat distance of $I_c = 9.36$ Å was obtained.[5] Chieu *et al.*[6] intercalated benzene-derived graphite fibers, heat treated to 2900 °C, and by characterizing these fiber samples using Raman scattering, they were able to demonstrate the presence of stage-1 $NiCl_2$-GIC within the optical skin depth of the fiber. To our knowledge, the present work is the first report of the magnetic properties of stage-1 $NiCl_2$-GIC's.

In this study, kish graphite , highly oriented pyrolytic graphite (HOPG), and natural flake graphite have been intercalated with $NiCl_2$; it was always easier to intercalate the thinner and smaller pieces of host material. The magnetic results shown in this paper were obtained using natural graphite flakes from Alfa Products, and each flake had a typical weight of 0.1 mg prior to intercalation. The intercalation reaction was carried out in a quartz ampoule and took 1–2 months, after which the samples were blue, typical of stage-1 acceptor compounds. The (00l) x-ray diffraction scan, Fig. 1, using Cu $K\alpha$ radiation shows that the single crystals are not pure stage-1, but are contaminated with weak stage-2 peaks [the (003) peak marked in Fig. 1 at $2\theta = 21.1°$ being particularly strong]. From the stage-1 peak positions, the

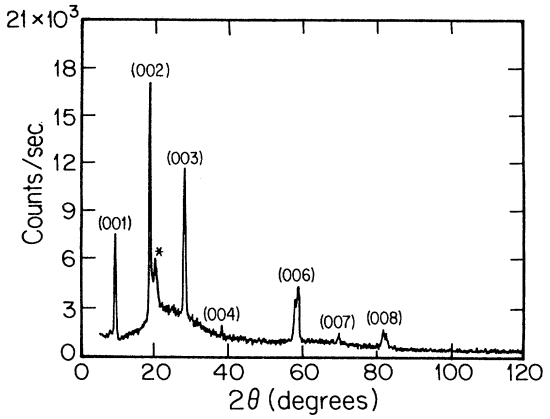

FIG. 1. (00l) x-ray diffraction scan of a mosaic array of stage-1 $NiCl_2$-GIC flakes, showing a small admixture of stage-2 through the presence of a (003) stage-2 reflection marked by the asterisk.

value $I_c = 9.36 \pm 0.05$ Å was obtained. The scans show little evidence of shifting or broadening of the x-ray peaks; such broadening effects would suggest random-layer stacking of the different stages according to the Hendricks-Teller model.[7]

X-ray precession studies of small single crystals have allowed us to elucidate the crystallography of this GIC system. Zero-level x-ray precession photographs recorded along **c** and **a** are shown in Fig. 2. These zero-level photographs represent two-dimensional "slices" of the reciprocal lattice (normal to the real-space-zone axis) which include the origin of reciprocal space. Upon intercalation, the $NiCl_2$ and graphite maintain their pristine in-plane symmetries and lattice constants within $\sim 1\%$. Hence the $NiCl_2$ layers are translationally incommensurate with respect to the carbon layers. The intercalate layer in stage-1 $NiCl_2$-GIC's (as with all of the incommensurate MCl_2-GIC's, where M denotes a metal atom) exhibits rotational epitaxy with $\mathbf{a}_{NiCl_2}$ centered about $\mathbf{a}_{graphite}$ with a FWHM linewidth of $\sim 4°$ as shown schematically in Fig. 2(c). This range of misorientation accounts for the circumferential arcing of the intercalate ($hk0$) reflections shown in Fig. 2(a).

The stacking sequence is determined by indexing precession photographs along the in-plane axes. To successfully index the a-axis precession photographs, a domain twin model must be incorporated to account for the fact that the three-dimensional intercalate structure possesses lower symmetry ($R\bar{3}m$) than an individual carbon (graphene) layer ($6mm$). Assuming that the $NiCl_2$ layers have $R\bar{3}m$ symmetry, there are two unique possible orientations of the intercalate layer. Using these two lattices, all of the intercalate reflections satisfy the condition $-h+k+l = 3m$, where m is an integer. These two sets of reflections are indicated in Fig. 2(d) by solid and partially closed circles in the schematic interpretation of the a-axis precession photograph. This condition results in rhombohedral ($\cdots \alpha\beta\gamma\alpha\beta\gamma \cdots$) stacking for the inter-

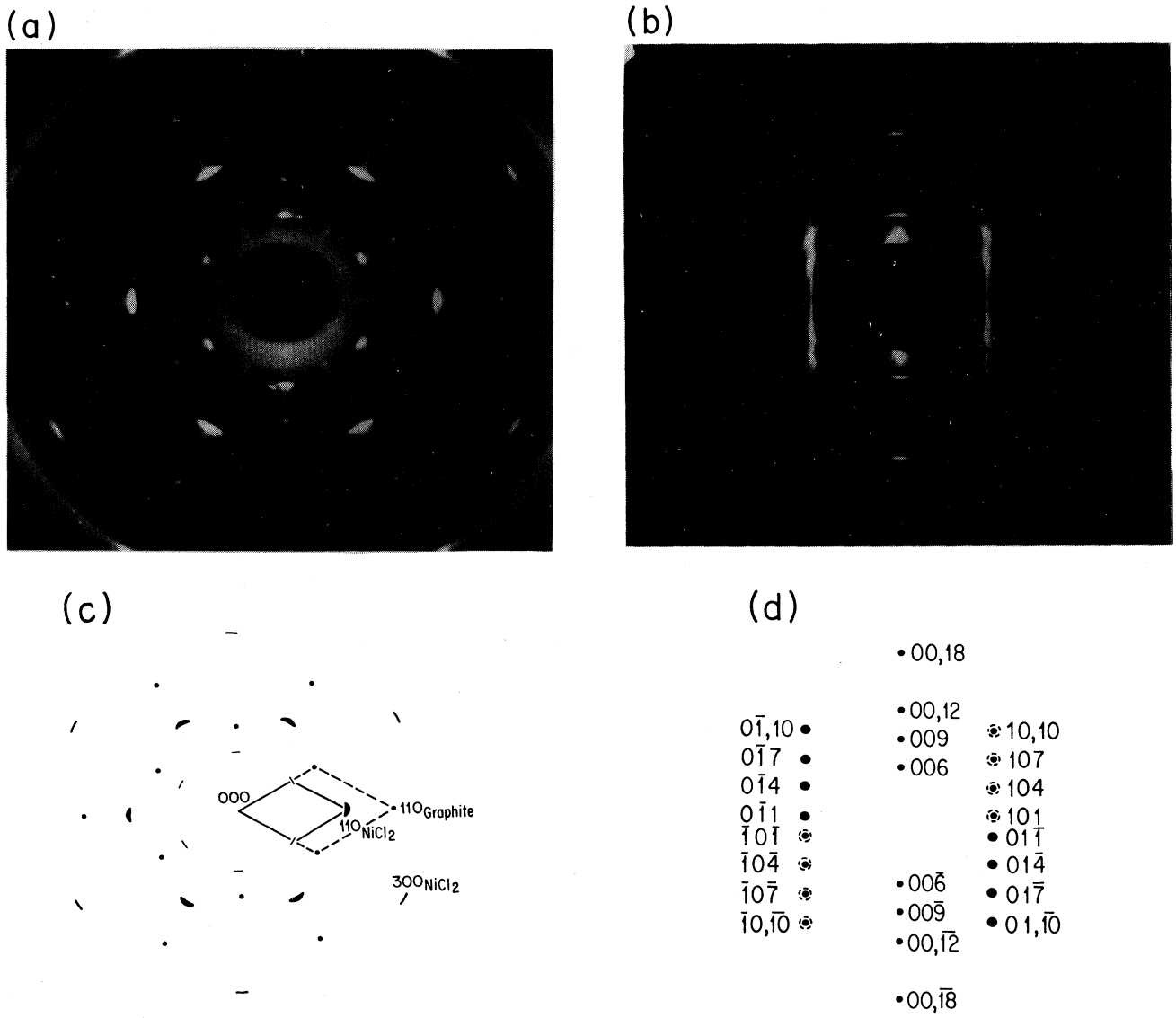

FIG. 2. Zero-level x-ray precession photographs from stage-1 $NiCl_2$-GIC (a) zone-axis along **c** and (b) zone-axis along **a**. (c) A schematic interpretation of the photograph (a) showing both the graphite and intercalate reciprocal unit cells. (d) Schematic interpretation of (b) showing the *hkl* reciprocal lattice point identifications. The indexing scheme used is that of the full three-dimensional lattice; hence the *l* values are three times larger than used in the indexing of Fig. 1. The large solid circles indicate *h*0*l* reciprocal lattice points from one of two possible intercalate orientations. The partially open circles indicate 0*kl* reciprocal lattice points from the other intercalate orientation.

calate layers, similar to the stacking in pristine $NiCl_2$. The diffuse nature of the intercalate (*h*0*l*) or (0*kl*) reflections in Fig. 2(b) is attributed to both the large mosaic spread in the crystal and the small 3D crystallographic coherence length. A more complete report of this structural work will be published elsewhere.[8]

Further evidence for 3D ordering of the intercalate layers comes from x-ray diffraction results measured on a four-circle diffractometer. In Fig. 3 we show a radial scan ($\theta-2\theta$) through the $(113)_{NiCl_2}$ peak (see inset of Fig. 3 for scan direction). The first peak encountered as 2θ increases is $(110)_{NiCl_2}$ at $2\theta=52.35°$. The shoulder on the high 2θ side of the $(110)_{NiCl_2}$ peak is the $(113)_{NiCl_2}$ peak ($2\theta=53.31°$). The large mosaic spread in the crystal smears the 110 and 113 reciprocal lattice points into spherical caps. A portion of the 110 spherical cap lies in the path of a vector connecting the origin of the reciprocal lattice to the center of the 113_{NiCl_2} reciprocal lattice position. Hence the first peak measured in a scan from the origin to 113_{NiCl_2} is the $(110)_{NiCl_2}$ peak. The scan in Fig. 3 clearly shows a distinct $(113)_{NiCl_2}$ peak. The presence of discrete (*hkl*) reflections is a clear indication of 3D ordering of the intercalate.

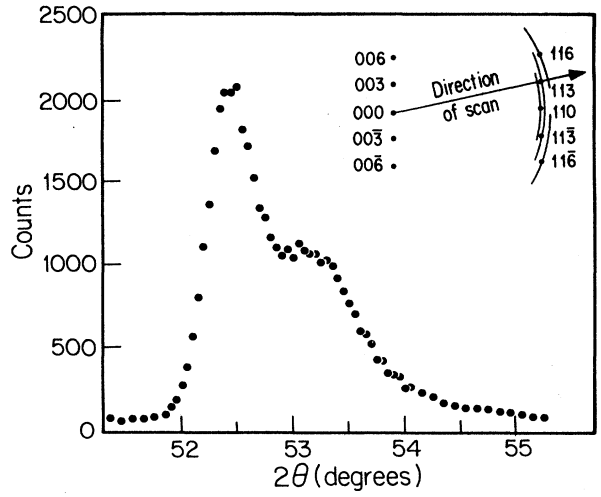

FIG. 3. Radial scan ($\theta-2\theta$) of single-crystal stage-1 $NiCl_2$-GIC through the 113_{NiCl_2} reciprocal lattice point. The inset shows the direction of the scan. The circumferential arcing of the reciprocal lattice points is due to the mosaic spread in the crystal. Because of the large mosaic spread of the crystal used for this experiment, the $(110)_{NiCl_2}$ peak is also measured in this scan (see text for further details).

Additional structural evidence for the existence of stage-1 $NiCl_2$-GIC was obtained from Raman characterization. Figure 4 shows a single Raman peak at 1624 cm^{-1}, with HWHM = 4.0 cm^{-1}; this spectrum was obtained from the edge of an HOPG-based sample, where the edge was visibly thicker than the rest of the sample. In the center of this sample, the Raman spectrum showed two peaks (1583 cm^{-1}, 1603 cm^{-1}) that are characteristic of a much higher stage ($n \geq 3$).[9] The first-order Raman peak centered at 1624 cm^{-1} occurs at a lower frequency than the Raman shift of 1633.5 cm^{-1} observed in the intercalated fibers,[6] but is still within the range of values that has been reported for several stage-1 acceptor compounds.[10]

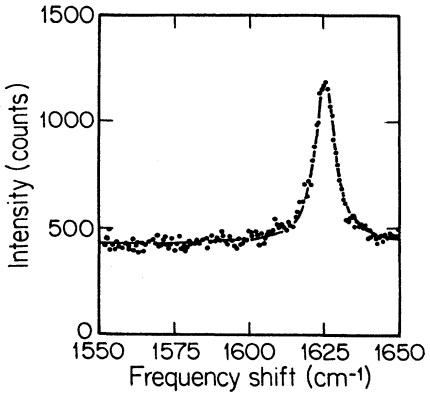

FIG. 4. Raman spectrum of a stage-1 region of a HOPG-based $NiCl_2$-GIC sample.

III. EXPERIMENTAL RESULTS

In-plane ac susceptibility measurements χ^{aa} were performed on a mosaic array of six intercalated natural graphite pieces mounted on a glass coverslip. The modulating field of amplitude 0.3 Oe, frequency 300 Hz, is parallel to the applied field **H**. The χ^{aa} versus T data, see Fig. 5, show a stage-1 shoulder at $T=23.0\pm0.5$ K. The much larger peak observed at $T=18.5$ K is the susceptibility maximum for the stage-2 $NiCl_2$-GIC's and higher stage regions of the sample. The higher-stage-susceptibility contributions are much stronger than the stage-1 contribution (even though the higher stages are minority phases as determined by x rays), because the susceptibility signal per Ni^{2+} ion increases rapidly with increasing stage number n. This conclusion is inferred from the rapid increase of the susceptibility maximum versus stage n that was observed in the $CoCl_2$-GIC's (Ref. 11) and in the $FeCl_3$-GIC's.[12] When the $\chi^{aa}(T)$ measurements on the $NiCl_2$-GIC sample (see Fig. 5) were repeated in the presence of a magnetic field, the lower-temperature peak was completely suppressed by a field of $H=300$ Oe. The upper peak was also slightly attenuated and this peak was shifted to a lower temperature ($\sim$22.0 K). Figure 6 shows a series of $\chi^{aa}(H)$ plots, the data being taken at different temperatures T. At $T=11.5$ K (plot *a*), the lowest temperature at which two peaks could be clearly observed, the field values of the maxima (interpreted as field-induced phase transitions) were $H_{c1}=380$ Oe and $H_{c2}=780$ Oe. As the temperature increases, the two transitions move towards lower field values, as shown in plots $b \rightarrow h$. These peak structures persist up to $T=21.4$ K (plot *i*), but disappear by $T=22.5$ K (plot *j*). In the low-field region $H<100$ Oe, we observed the susceptibility contribution of the stage-2 regions of the samples; here there were low field transitions, as were previously observed by Suzuki *et al.*[13] The low field transi-

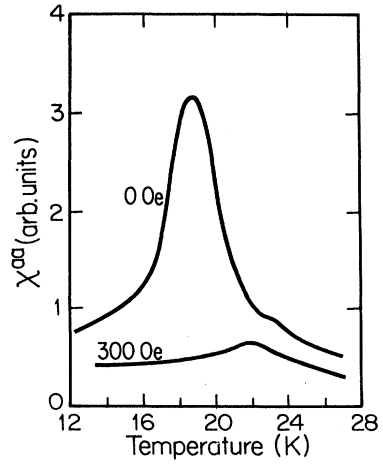

FIG. 5. $\chi^{aa}(T)$ data for the nominal stage-1 $NiCl_2$-GIC sample showing a stage-1 maximum at 23 K and a stage-2 (and higher stage) peak at about 18 K. The lower temperature peak can be essentially eliminated by the application of a field of 300 Oe.

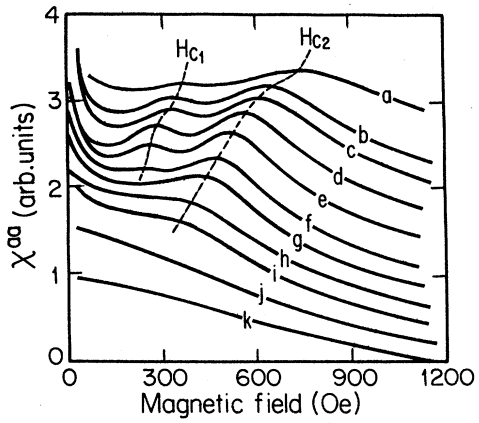

FIG. 6. In-plane ac susceptibility χ^{aa} vs H of a mosaic of stage-1 $NiCl_2$-GIC samples at different temperatures: *a*, 11.5 K; *b*, 16.1 K; *c*, 16.9 K; *d*, 17.8 K; *e*, 18.8 K; *f*, 19.7 K; *g*, 20.2 K; *h*, 21.2 K; *i*, 21.4 K; *j*, 22.5 K; *k*, 23.3 K. No demagnetization corrections were made, and the traces in the figure are displaced so that the various sweeps do not overlap. The peaks H_{c1} and H_{c2} are indicated.

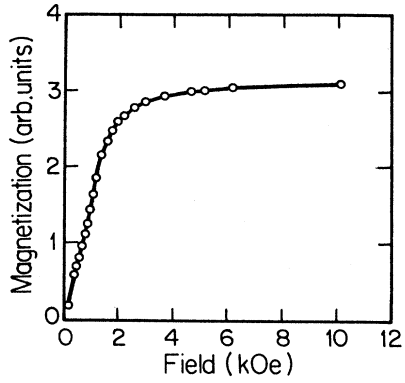

FIG. 8. SQUID magnetization trace taken at $T=7.5$ K on the same mosaic sample as in Fig. 6.

tions in our traces disappeared at $T\sim 20$ K. Unfortunately, there are no field traces reported above 19.4 K for stage-2 $NiCl_2$-GIC's (Ref. 13) with which we can compare our data.

The values of H_{c1} and H_{c2} as a function of temperature T are plotted as a phase diagram in $H-T$ space, as shown in Fig. 7. Similar susceptibility results were obtained for larger HOPG-based nominal stage-1 samples, for which an overall stronger signal was obtained, but the HOPG samples showed proportionally larger stage-2 regions. The size of the anomaly at H_{c1} was also found to be relatively smaller in the HOPG-based samples.

Magnetization measurements, Fig. 8, were also carried out, using the SQUID magnetometer at the Francis Bitter National Magnet Laboratory. The measurements of $M(\mathbf{H}\perp\mathbf{c})$ confirm the $\chi^{aa}(H)$ measurements presented in Fig. 6 and check that there are no higher field transitions (up to 10 kOe) than those accessible in the susceptibility experiment. For $T=7.5$ K the in-plane magnetization saturated at ~ 3 kOe.

Magnetotransport experiments were carried out on a single flake of $NiCl_2$ intercalated natural graphite with an area of about 1 mm^2. The standard four-probe method was used; a dc current of 1 mA was used and the magnetic field was applied in the x-y plane. There was no noticeable difference in the transport results when, keeping $\mathbf{H}\perp\mathbf{c}$, the geometry was changed from ($\mathbf{j}\|\mathbf{H}$) to ($\mathbf{j}\perp\mathbf{H}$), where $\mathbf{j}$ is the current density. Although the transport measurements are sensitive to scattering contributions from differently staged parts of the sample, the magnetic scattering contributions to the transport properties of a pure stage-2 sample were measured to be less than the experimental noise level, so we assume that the stage-1 $NiCl_2$-GIC is the predominant magnetic scatterer of conduction electrons in our mixed phase sample.

In the zero-field resistivity trace shown in Fig. 9, the temperature T was swept from 30 to 5 K. The most striking feature of the zero-field data is the sharp increase of the resistivity for temperatures less than 21.5 K. The magnitude of the maximum scattering from the magnetic

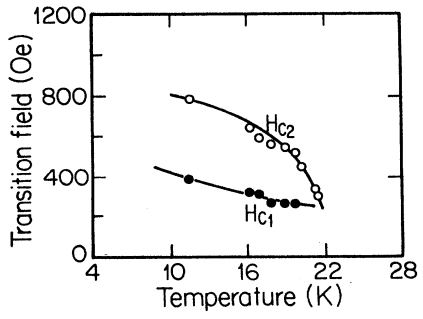

FIG. 7. The H-T phase diagram derived from $\chi^{aa}(H)$ data, showing data points for the H_{c1} and H_{c2} transitions. The solid lines are a guide to the eye.

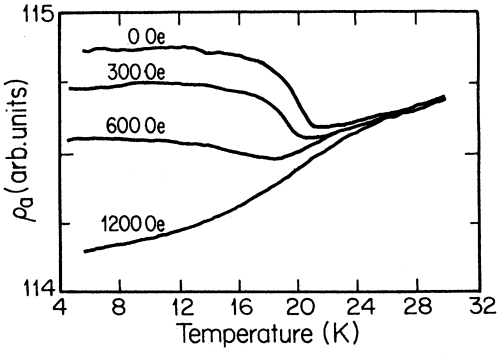

FIG. 9. Resistivity ρ_a vs temperature T of a single flake of intercalated (stage-1 $NiCl_2$ GIC) natural graphite in applied in-plane magnetic fields of 0, 300, 600, and 1200 Oe.

species compared to the "background" resistivity [$\rho_a = a + bT + cT^2$ is expected for typical nonmagnetic GIC's (Ref. 14)] $\Delta\rho_a/\rho_a$ varies from 1% to 10%, depending on the sample. The most likely cause of this variation is the lack of homogeneity in the samples and the resultant mixing of ρ_a and ρ_c. The previously mentioned sharp increase in resistivity can be reduced by application of a magnetic field, e.g., at 600 Oe, the size of $\Delta\rho_a/\rho_a$ at low temperatures is halved. In a field of 1200 Oe, the magnetic scattering is nearly quenched. Figure 10 shows field sweeps for $\rho_a(H)$ at different temperatures. The data have been displaced to show clearly that upon approaching $T=21.5$ K the magnetoresistance becomes flatter. Within experimental error, the traces at $T=21.6$ K (trace *k*) and $T=21.9$ K (trace *l*) are identical, from which we conclude that $T_N \sim 21.5$ K at a field of ~ 300 Oe. Furthermore, T_N predicted in this way is lower than for the $H=0$ experiments because T_N depends on H. This behavior is consistent with the H-T phase diagram in Fig. 7 and with the magnetic field-induced shift in the peak in $\chi^{aa}(T)$ shown in Fig. 5.

The field dependence of the resistivity $\rho_a(H)$, at fixed temperature T, has fewer features than the corresponding susceptibility $\chi^{aa}(H)$ traces. We can define the transition field H_t as the point at which $|\partial\rho_a/\partial H|$ is maximum in the traces of Fig. 10; this maximum is shown for $T=4.2$ K in the lower half of Fig. 11 in relation to the $\rho_a(H)$ trace shown in the upper half of the figure. The values of H_t thus obtained for different temperatures are plotted in Fig. 12. The resistivity (in the upper half of Fig. 11) is found to be featureless above 3 kOe, a field value that can be interpreted as the saturation field H_{sat}.

IV. DISCUSSION

In all the transition-metal chloride GIC's investigated to date, the intercalate does not completely fill the layers between the graphite sheets;[3,8] we assume that the stage-1 $NiCl_2$-GIC's are no exception. The in-plane lattice constants of pristine $NiCl_2$ and $CoCl_2$ (both have the $CdCl_2$ structure) differ by less than 0.5% and the rotational epitaxy angles and layer-stacking arrangements for stage-1 $NiCl_2$-GIC's are the same as for stage-1 $CoCl_2$-GIC's. The consistency of these structural results with other transition metal MCl_2-GIC's is explained elsewhere.[8,15] The value of the repeat distance $I_c = 9.36 \pm 0.05$ Å is consistent with the I_c(stage-2) $= 12.67 \pm 0.03$ Å result[13] and application of the formula $I_c = (n-1)c_0 + d_s$, where $d_s = I_c$(stage-1), n is the stage number, and $c_0 = 3.35$ Å. Our value of I_c also agrees with that obtained by Stumpp.[5]

The magnetic properties of stage-1 $NiCl_2$-GIC's are expected to lie between those of pristine $NiCl_2$ and stage-2 $NiCl_2$-GIC's. The Hamiltonian for pristine $NiCl_2$ may be

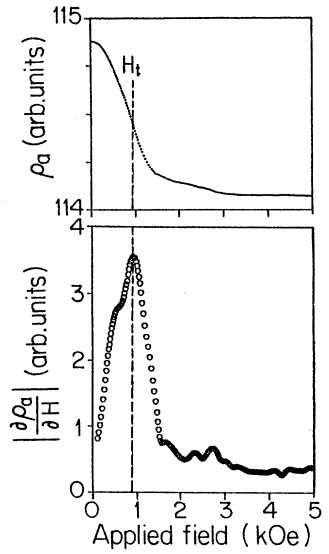

FIG. 11. The resistivity and its derivative at $T=4.2$ K as a function of magnetic field.

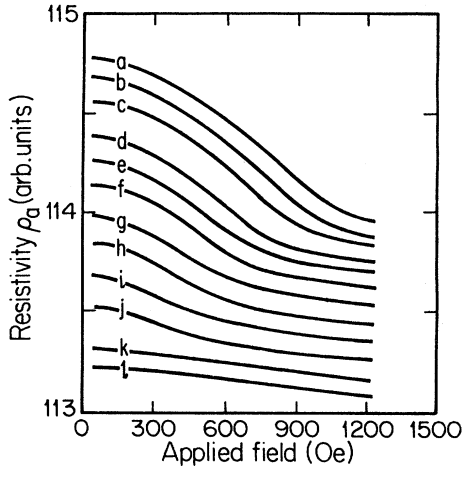

FIG. 10. In-plane resistivity $\rho_a(H)$ of intercalated (stage-1 $NiCl_2$-GIC) natural graphite single crystal at various temperatures: *a*, 4.2 K; *b*, 9.4 K; *c*, 12.2 K; *d*, 16.4 K; *e*, 17.8 K; *f*, 18.7 K; *g*, 19.5 K; *h*, 20.0 K; *i*, 20.4 K; *j*, 21.0 K; *k*, 21.6 K; *l*, 21.9 K.

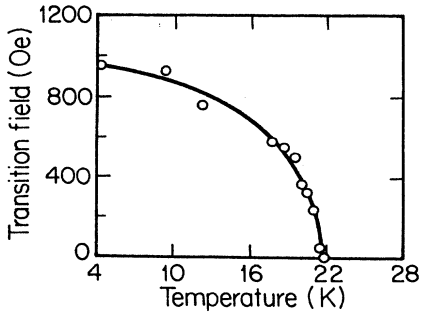

FIG. 12. The H-T phase diagram derived from $\rho_a(H)$ data, showing data points for the H_t transition. The solid line is a guide to the eye. Note the similarity of the H_t values compared with those of H_{c2} shown in Fig. 7.

written in the form[16]

$$\mathcal{H}=-2J\sum_{i>j}\mathbf{S}_i\cdot\mathbf{S}_j-2J'\sum_{i>k}\mathbf{S}_i\cdot\mathbf{S}_k+D\sum_i(S_{iz}^2-S_{ix}^2-S_{iy}^2)\ , \tag{1}$$

where the index j (k) is over nearest-neighbor intraplanar (interplanar) spins, and $|\mathbf{S}|=1$. The values $J=21.7$ K, $D=0.4$ K, and $J'=-0.8$ K have been measured for pristine $NiCl_2$ by magnetization[17,18] and neutron scattering[16] experiments. This Hamiltonian [Eq. (1)] was used to describe stage-2 $NiCl_2$-GIC's,[19] which show quasi-two-dimensional behavior at $JS^2/k_B\approx 20$ K, suggesting that J (and other in-plane magnetic properties) is not strongly affected by intercalation. The value of the anisotropy of the g value, $g_{aa}-g_{cc}=2.156-2.096=0.06$ obtained in the stage-2 compound[19] gives rise to a calculated anisotropy (using the theory of Lines[20] as a rough estimate) of $D/J=0.021$, close to that of the pristine material (0.018) and suggesting XY behavior. It is expected that a similar value for D/J will be found in the intermediate stage-1 compounds, and it is further assumed that the above Hamiltonian will also describe stage-1 $NiCl_2$-GIC's. The only stage-dependent quantity in $\mathcal{H}$ is the antiferromagnetic interaction J', which we estimate below.

The zero-field susceptibility peak at $T=23$ K occurs at a higher temperature than any other magnetic feature observed in the ac susceptibility of the stage-2 compounds.[13] The relatively weak sensitivity of the magnitude of the 23 K peak to an applied field (see Fig. 5) supports its identification with the stage-1 phase of the sample. We can tentatively interpret the Néel temperature T_N as being close to 23 K; the peak structure in $\chi^{aa}(H)$ and in $|\partial\rho_a/\partial H|$ disappears at 22.0 ± 0.5 K. This is usual behavior for a conventional antiferromagnet, i.e., the temperature of the ac susceptibility maximum is found to be higher than the actual 3D ordering temperature as determined by neutron scattering. Within the accuracy of our susceptibility and resistivity experiments, we obtain $T_N=22.0\pm0.5$ K for stage-1 $NiCl_2$-GIC's. By comparison, the susceptibility maximum in stage-1 $CoCl_2$-GIC's also occurs at higher temperatures than the maxima of the higher-stage $CoCl_2$-GIC's.

In interpreting the magnetic field results, we know that the minority stage-2 phase is saturated at fields above 100 Oe.[13,21] The phase transitions that we observe at H_{c1} and H_{c2} are too high in field to be confused with stage-2 (or higher stage) effects and are too small in field to be caused by pristine $NiCl_2$. In the 3D ordered phase of this system, we would expect a number of transitions when a magnetic field is applied in the x-y plane. In zero field, the system is an antiferromagnet (AF); at a certain field the antiferromagnetic phase flops into the spin-flop (SF) phase, where the spins on alternate layers are aligned at angles of $\pm\pi/3$ with respect to the magnetic field applied along an easy direction.[22] At even higher fields, there will be an eventual alignment of the spins along the applied field, leading to the spin-aligned paramagnetic (P) phase. The ratio $H_{c2}/H_{c1}\approx 2$ is similar to that observed in stage-1 $CoCl_2$-GIC's (300/160) (Ref. 22) and in stage-2 $NiCl_2$-GIC's (25/15) (Ref. 13) but cannot be explained by the mean-field theory proposed by Szeto *et al.*,[22] where the ratio $H(\mathrm{SF}\rightarrow P)/H(\mathrm{AF}\rightarrow\mathrm{SF})$ is 3.0 at $T=0$ K. A value of 3 for this ratio is also found by Monte Carlo simulations.[23] The peak structure at H_{c1} in χ^{aa} versus H for stage-1 $CoCl_2$-GIC's is not observed in all samples; later work on better characterized samples found the peak at H_{c2} to be more dominant. The strong sample dependence of the H_{c1} structure in both stage-1 $NiCl_2$ and $CoCl_2$-GIC's is not well understood, but may be due to the range of angles of the easy axes on the various magnetic layers with respect to the applied magnetic field.

To estimate the magnitude of the antiferromagnetic coupling J' we shall ignore the low field structure and assume that the in-plane anisotropy is small compared to J'. We can estimate the magnitude of J' from the saturation field, which is the field that is required, at $T=0$ K, to overcome the antiferromagnetic interplanar coupling, and is given by

$$H_{\mathrm{sat}}\approx zJ'S/g_{aa}\mu_B\ , \tag{2}$$

where μ_B is the Bohr magneton. The number of next nearest neighbors on adjacent Ni^{2+} layers, $z=12$, is the same for both the stage-1 and pristine compounds. From our studies of the magnetization $M(H)$ and resistivity $\rho_a(H)$, we estimate that $H_{\mathrm{sat}}=3.0$ kOe for stage-1 $NiCl_2$-GIC's, and hence the value of $|J'/J|=1.5\times10^{-3}$

TABLE I. Comparison between the properties of stage-1 and stage-2 $NiCl_2$-GIC's and pristine $NiCl_2$.

Compound	Pristine $NiCl_2$	Stage-1 $NiCl_2$-GIC	Stage-2 $NiCl_2$-GIC
Interlayer distance[a]	5.73±0.05 Å	9.36±0.05 Å	12.67±0.03 Å
$NiCl_2$ stacking	rhombohedral	rhombohedral	random
θ[b]	–	0°±2°	0°±2°
T_N	54.5 K	22.0±0.5 K	$T_{cl}=19.5$ K[c]
$H_{c1}(0)$	–	380 Oe	15 Oe[c]
$H_{c2}(0)$	–	780 Oe	25 Oe[c]
$H_{\mathrm{sat}}(0)$	–	3 kOe	100 Oe[c]
$\lvert J'/J\rvert$	0.037	1.5×10^{-3}	5.1×10^{-5}

[a]Interlayer distance denotes the separation between consecutive Ni^{2+} layers.
[b]Rotational epitaxy angle.
[c]Reference 13.

given in Table I can be calculated. In the same table this ratio is estimated for stage-2 $NiCl_2$-GIC's assuming that $H_{sat}=100$ Oe.[13] The ratio of J'(pristine)/J'(stage-1) is ~ 30 for both $NiCl_2$ and $CoCl_2$-GIC's, suggesting that a similar mechanism is responsible for the reduction of J' in both stage-1 compounds. If we extrapolate our reasoning to the stage-2 compounds, using J'(pristine)/J'(stage-2)$=720$ for stage-2 $NiCl_2$-GIC's we estimate that J'(stage-2 $CoCl_2$)$=0.003$ K, close to the value obtained from high-temperature susceptibility measurements,[24] $J'=0.007$ K.

The transport properties of stage-1 $NiCl_2$-GIC's are very similar to their stage-1 $CoCl_2$ counterparts,[25] where a careful comparison between $\chi^{aa}(H)$ and $\rho_a(H)$ shows that $\rho_a(H)$ is only sensitive to the transition at H_{c2}; no detailed comparison was carried out in Ref. 25. Figure 7 (susceptibility) and Fig. 12 (magnetoresistance) show similar behavior for the temperature dependence of H_{c2} in stage-1 $NiCl_2$-GIC's.

The resistivity behavior can be explained by a model that accounts for the additional periodicity introduced in the k_z direction by the antiferromagnetic ordering along the c axis; this causes a Fermi surface distortion that affects the transport properties. The theory was originally developed to explain resistance anomalies in the rare-earth metals,[26] and predicts that

$$1/\rho_a=\sigma_a=\sigma_a(0)[1+O(\Delta/E_F)^2] \quad (3)$$

and

$$1/\rho_c=\sigma_c=\sigma_c(0)[1-O(\Delta/E_F)] , \quad (4)$$

where Δ is the new energy gap introduced at the Fermi level E_F due to the AF order, and $\sigma_a(0)$ and $\sigma_c(0)$ are the a- and c-axis conductivities of the unperturbed system without Fermi-surface distortions. In the usual case we have $\Delta/E_F \ll 1$, and the change in σ_c will be much larger than the change in σ_a. If there is strong mixing of σ_a and σ_c by staging defects or other inhomogeneities, then this theory may account for the unusual magnetic behavior observed in ρ_a. However, if the experimental measurements of ρ_a are precisely in-plane, and if ρ_a increases anomalously below T_N (as indicated in Fig. 9), then the theory of Sugihara *et al.*[25] may be more suitable. Whichever theory is correct, both require long-range antiferromagnetic order along the c axis, a condition that is satisfied by stage-1 $CoCl_2$-GIC's.[1] The transport results suggest a similar long-range magnetic order in stage-1 $NiCl_2$-GIC's; however, neutron scattering measurements are needed to confirm this conjecture.

A number of factors may be responsible for the purely three-dimensional magnetic behavior of $NiCl_2$ and $CoCl_2$ stage-1 compounds compared to the quasi-two-dimensional behavior of their respective stage-2 compounds. First J'(stage-2) is reduced relative to J'(stage-1) because the distance between the metal-ion layers is increased due to the presence of an extra graphite layer. Second, these properties depend on the enhancement of the interplanar antiferromagnetic interaction in the stage-1 compound relative to stage-2 due to the in-plane spin-correlation length ξ_a through the formula

$$J'S^2(\xi_a/a)^2 \sim k_B T_N , \quad (5)$$

where T_N is the 3D ordering temperature and a is the distance between adjacent spins in the x-y plane. For stage-1 $NiCl_2$-GIC's and $CoCl_2$-GIC's we estimate J' from H_{sat}; from Eq. (5), this gives ξ_a values of 90 and 40 Å, respectively. For the stage-2 $CoCl_2$-GIC's, ξ_a saturates at 900±150 Å for $T<T_{cu}$,[27] and the value of ξ_a calculated from Eq. (5) for a stage-2 $NiCl_2$-GIC is of the same order, i.e., 480 Å. These effects are under further investigation.[8]

V. CONCLUSIONS

In conclusion we have prepared stage-1 $NiCl_2$-GIC's and have characterized their magnetic and structural properties. We have found a large number of similarities between stage-1 $NiCl_2$-GIC's and stage-1 $CoCl_2$-GIC's. They both exhibit rhombohedral stacking of the intercalate layers which are oriented at 0° with respect to the graphite **a** axes. This structural three dimensionality also affects the magnetic behavior.

Magnetically the two compounds appear to undergo a transition to an ordered 3D antiferromagnetic state. For $T<T_N$, this gives rise to field-induced transitions and strong conduction-electron scattering. We have also obtained a measure of how the interplanar coupling J' decreases upon intercalation and a measure of the stage dependence of J'.

ACKNOWLEDGMENTS

This work was supported by U.S. Air Force Office of Scientific Research (AFOSR) Contract Grant No. F49620-83-C-0011 in its initial stages and by National Science Foundation (NSF) Grant No. DMR-83-10482 thereafter. We are grateful to Professor M. S. Dresselhaus for her comments and encouragement, and we thank Dr. G. L. Doll for carrying out the Raman characterization. Additionally, we thank Professor R. W. Balluffi and Dr. I. Majid for the use of their four-circle diffractometer.

[1] H. Ikeda, Y. Endoh, and S. Mitsuda, J. Phys. Soc. Jpn. **54**, 3232 (1985).

[2] D. G. Wiesler, M. Suzuki, and H. Zabel, Phys. Rev. B **36**, 7051 (1987).

[3] S. Flandrois, J. M. Masson, J. C. Rouillon, J. Gaultier, and C. Hauw, Synth. Met. **3**, 1 (1981).

[4] G. Chouteau and R. Yazami, Europhys. Lett. **3**, 229 (1987).

[5] E. Stumpp, in *Proceedings of the International Colloquium on Layered Compounds, Pont-à-Mousson,* 1988, edited by D. Guérard and P. Lagrange (unpublished), p. 41.

[6] T. C. Chieu, G. Timp, M. S. Dresselhaus, and M. Endo in, *Proceedings of the Symposium on Intercalated Graphite,* edited by M. S. Dresselhaus, G. Dresselhaus, J. E. Fischer, and M. J. Moran (North-Holland, Amsterdam, 1983), p. 51.

[7] M. E. Misenheimer and H. Zabel, Phys. Rev. Lett. **54**, 2521 (1985).

[8]J. S. Speck, J. T. Nicholls, B. J. Wuensch, and M. S. Dresselhaus (unpublished).

[9]M. S. Dresselhaus and G. Dresselhaus, in *Light Scattering in Solids III,* edited by M. Cardona and G. Güntherodt (Springer-Verlag, Berlin, 1982), p. 3.

[10]M. S. Dresselhaus, G. Dresselhaus, K. Sugihara, I. L. Spain, and H. A. Goldberg, in *Graphite Fibers and Filaments,* Vol. 5 of *Springer Series in Materials Science* (Springer-Verlag, Berlin, 1988).

[11]M. Elahy and G. Dresselhaus, Phys. Rev. B **30**, 7225 (1984).

[12]A. K. Ibrahim and G. O. Zimmerman, Phys. Rev. B **35**, 1860 (1987).

[13]M. Suzuki and H. Ikeda, J. Phys. C **14**, L923 (1981).

[14]M. S. Dresselhaus and G. Dresselhaus, Adv. Phys. **30**, 139 (1981).

[15]J. S. Speck, B. J. Wuensch, and M. S. Dresselhaus, in *Extended Abstracts of the Symposium on Graphite Intercalation Compounds at the Materials Research Society Meeting, Boston,* edited by M. Endo, M. S. Dresselhaus, and G. Dresselhaus, (Materials Research Society, Pittsburgh, 1988), p. 29.

[16]P. A. Lindgard, R. J. Birgeneau, J. Als-Nielsen, and H. J. Guggenheim, J. Phys. C **8**, 1059 (1975).

[17]D. Billerey, C. Terrier, A. J. Pointon, and J. P. Redoules, J. Magn. Magn. Mater. **21**, 187 (1980).

[18]J. de Gunzbourg, S. Papassimacopoulos, A. Miedan-Gros, and Y. Allain, J. Phys. (Paris) **32**, CI125 (1971).

[19]M. Suzuki, K. Koga, and Y. Jinzaki, J. Phys. Soc. Jpn. **53**, 2745 (1984).

[20]M. E. Lines, Phys. Rev. **131**, 546 (1963).

[21]H. Suematsu, R. Nishitani, R. Yoshizaki, M. Suzuki, and H. Ikeda, J. Phys. Soc. Jpn. **52**, 3874 (1983).

[22]K. Y. Szeto, S. T. Chen, and G. Dresselhaus, Phys. Rev. B **33**, 3453 (1986).

[23]S. T. Chen, Ph.D. thesis, Massachusetts Institute of Technology, 1985 (unpublished).

[24]D. G. Wiesler, M. Suzuki, P. C. Chow, and H. Zabel, Phys. Rev. B **34**, 7951 (1986).

[25]K. Sugihara, N.-C. Yeh, M. S. Dresselhaus, and G. Dresselhaus, Phys. Rev. B **39**, 4577 (1989).

[26]R. J. Elliott and F. A. Wedgewood, Proc. R. Soc. London **81**, 846 (1963).

[27]D. G. Wiesler and H. Zabel, Phys. Rev. B **36**, 7303 (1987).

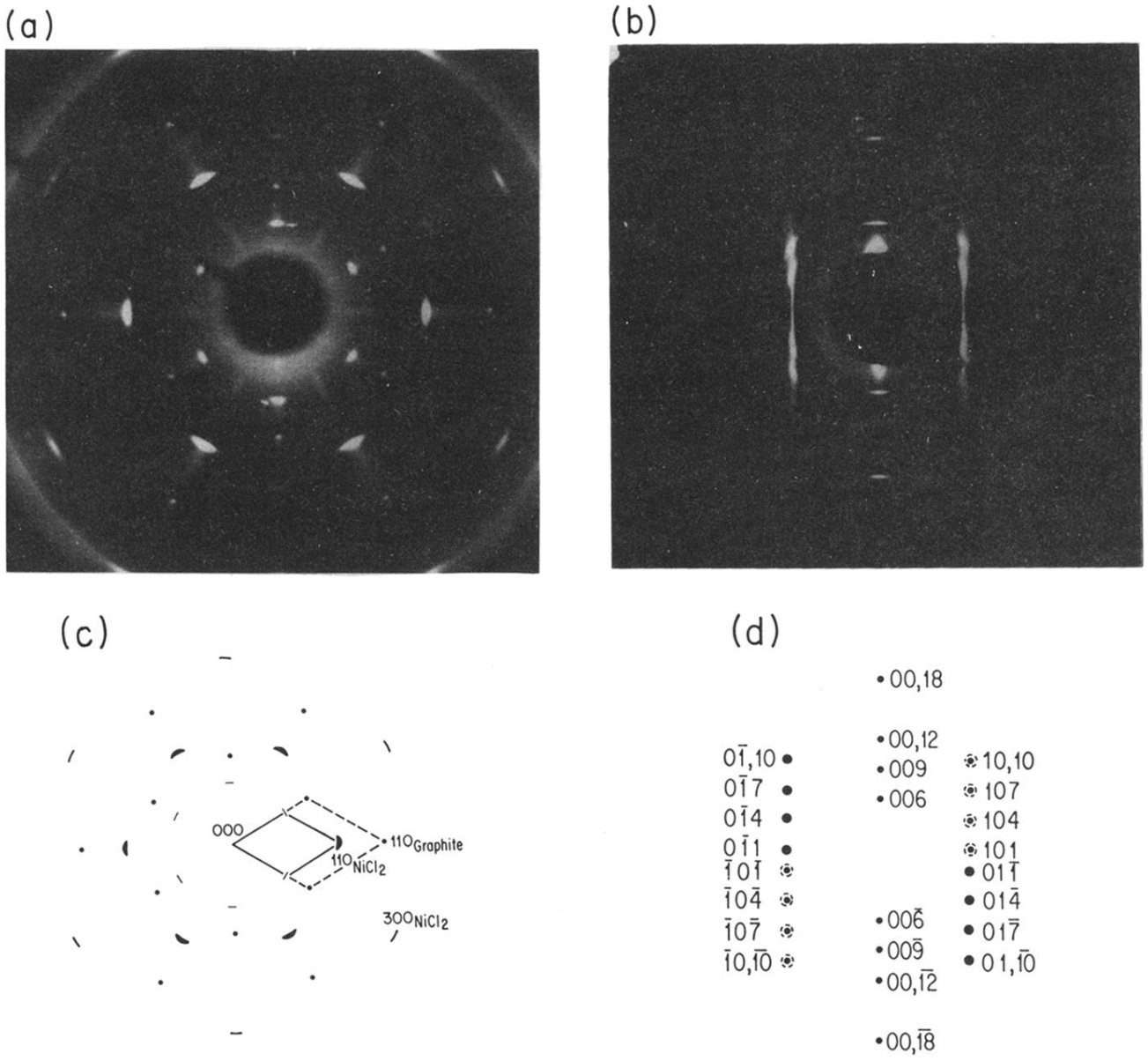

FIG. 2. Zero-level x-ray precession photographs from stage-1 $NiCl_2$-GIC (a) zone-axis along **c** and (b) zone-axis along **a**. (c) A schematic interpretation of the photograph (a) showing both the graphite and intercalate reciprocal unit cells. (d) Schematic interpretation of (b) showing the *hkl* reciprocal lattice point identifications. The indexing scheme used is that of the full three-dimensional lattice; hence the *l* values are three times larger than used in the indexing of Fig. 1. The large solid circles indicate *h*0*l* reciprocal lattice points from one of two possible intercalate orientations. The partially open circles indicate 0*kl* reciprocal lattice points from the other intercalate orientation.